Optical Properties, Electronic Structure, and Exciton Binding Energies in Short Period ZnS-ZnSe Superlattices

T. CLOITRE, L. AIGOUY, M. DI BLASIO, B. GIL, P. BIGENWALD, N. BRIOT, O. BRIOT, D. BOUCHARA, M. AVEROUS, and R.L. AULOMBARD

Université Montpellier II-Groupe d'Etudes des Semiconducteurs, Case Courrier 074–34095 Montpellier Cedex 5 - France

We present a detailed examination of the optical properties and electronic structure taken from photoreflectance and photoluminescence data collected on a series of short-period ZnS-ZnSe superlattices grown by low pressure metalorganic vapor phase epitaxy. We studied the band offset problem and calculated the exciton binding energy using several variational models. The temperature dependence of the photoluminescence properties of these superlattices was analyzed in the context of a model which includes the influence of the interfacial disorder.

Key words: II-VI wide bandgap semiconductors, built-in strain, exciton-related phenomena, photoluminescence characterization, superlattices

INTRODUCTION

ZnS-ZnSe superlattices display optical bistability[1,2] are potential candidates to the realization of devices based on Cerenkov-like second harmonic generation[3] and they may be used to filter defects at the GaAs-II-VI interface in ZnSe based light-emitters, or as a material used to confine photons in graded index separate confinement heterostructures (GRINSCH).[4] Short period ZnS-ZnSe strained-layer superlattices (SLSs) have been grown by metalorganic vapor phase epitaxy (MOVPE) using tetramethylmethylenediamine: dimethylzinc adduct (TMMD:DMZn). We will study their optical and electronic properties in this paper. These superlattices are grown as 45 repeats of a basic building block, where the thickness of the well and barrier layers are varied from some 10Å up to some 35Å. The following optical experiments were performed: reflectivity, photoreflectance, and photoluminescence at pumped liquid helium temperature (2K). From these experiments, we could detect the signatures of the heavy-hole and light-hole excitons. For a constant barrier width, and by decreasing the well width, the spectra is blue shifted, whereas, when the well width is held constant and the barrier width is decreased we can observe a red shift. This is consistent with the type I conduction to valence band configuration. Using a marginal conduction band offset in an elementary envelope function calculation has provided us a fairly good correlation between the theoretical and experimental data revealed. Better agreement has been obtained after a calculation of the exciton binding energies has been performed in the context of a sophisticated model which includes the deformation of the electron potential due to the hole density of charge. In this self-consistent calculation, we have included the electrostatic deformation of the marginal electron potential produced by the presence of a localized hole wave function. This reinforces the oscillator strength with respect to what we obtain when performing more conventional calculations of the exciton binding energy in low dimensional semiconductor systems. The asymmetry of the photoluminescence band has been interpreted in terms of exciton localization to interfacial potential fluctuations.

(Received June 28, 1994; revised December 2, 1994)

CRYSTAL GROWTH

The samples were grown by low pressure MOVPE in an ASM OMR 12 equipment. Hydrides were used as sulphur and selenide sources. Rather than using the "classical" zinc precursor, dimethylzinc, which is

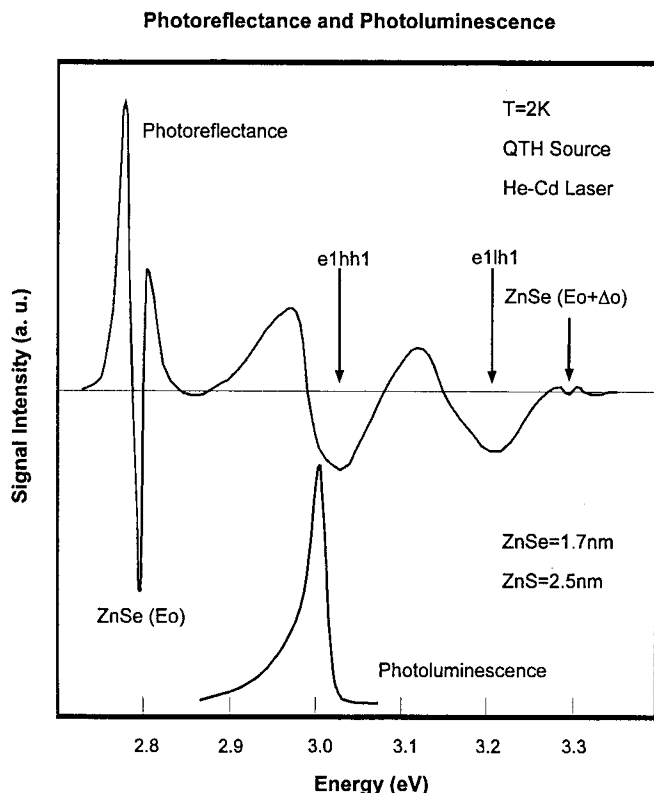

Fig. 1. Photoreflectance (top) and photoluminescence (bottom) of a ZnSe-ZnS superlattice grown on a GaAs substrates with a 3000Å ZnSe buffer layer.

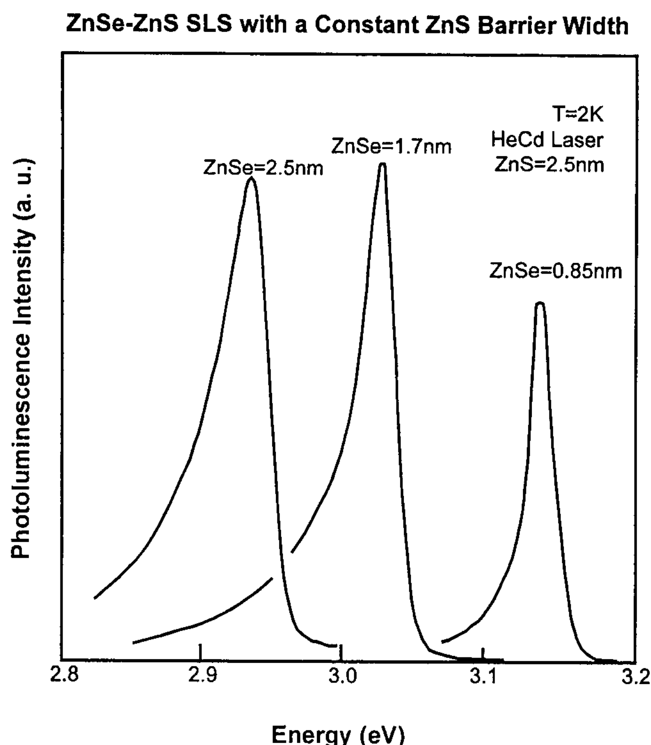

Fig. 2. Photoluminescence spectra taken at 2K which display the blue-shift of the emitted photon when the width of the ZnSe layers decreases.

always contaminated by traces of halides originating from the synthesis of the precursors, we used a novel molecule recently synthesized by Epichem Ltd. This molecule, TMMD:DMZn, gives even better results than the dimethylzinc triethylamine adduct (Me_2Zn:Net_3) that we used previously for growing such superlattices.[5] This is linked to the larger decrease of premature reactions and a better layer uniformity and surface morphology. Extensive details about this can be found in the paper of Briot et al.[4] The growth conditions were a growth temperature of 300°C, a reactor pressure of 40 Torr, and a VI/II ratio of 5. The superlattices were grown after a 3000Å ZnSe buffer layer was grown on a (001)-oriented GaAs epiready substrate. Growth interruption of 10 s at each heterointerface was found to improve the interface abruptness (better x-ray data and narrower photoluminescence lines). Period and mean lattice parameter were deduced from the observation of satellite peaks up to the second order in x-ray diffraction spectra. A modeling of the data including strain state (matching to the buffer or free-standing) was done to extract the thickness of individual layers. Due to the large lattice mismatch between ZnS and ZnSe bulk zinc-blende semiconductors (~4%), samples with low dislocation densities could only be grown for individual layer thickness below 40Å.

OPTICAL CHARACTERIZATION

Figure 1 displays a typical photoreflectance spectrum given by such superlattices. As a matter of comparison, the photoluminescence data has been also reported which shows the moderate stokes shift between the emission and creation processes. The photoreflectance spectrum is rather detailed and respectively shows from low to high energies: the signature of the E_0 transition in the ZnSe buffer, superlattice-related features corresponding to excitonic transitions involving the first confined electron state and the first heavy-hole and light-hole valence confined states respectively, and last the $E_0 + \Delta_0$ transition in the ZnSe buffer. These spectroscopic data analyzed in the context of the effective mass theory (envelope function approach)[6] are consistent with a free-standing model of strain state in the individual layers deduced from the x-ray data.

To show the evolution of the superlattices transition as a function of the modifications of the layer thickness, we report photoluminescence data. Figure 2 displays the evolution of the photoluminescence lines when changing the thickness of the ZnSe layer and keeping constant the thickness of the ZnS layers. We observe a blue-shift of the photoluminescence energy when decreasing the thickness of ZnSe, and a simultaneous increase of the full width at half maximum from 24 up to 42 meV via 32 meV. We also note the systematic existence of a low energy tail in these samples, and in samples of comparable crystalline quality that have been published by other groups.[7–22] From extensive studies previously made on GaAs(Ga,Al)As combination,[23,24] we conclude that

existence of this tail is linked to the interface morphology in ZnS-ZnSe superlattices. Interface imperfections such as randomly distributed islands or terraces have been frequently observed in heterostructures. The resulting photoluminescence line shape depends on the relative size of these terraces compared with the exciton Bohr diameter. Split sharp lines corresponding to one monolayer fluctuation of width or broad photoluminescence lines have been observed when the Bohr diameter is smaller or comparable to the terrace lateral extension. In our case, transmission electron microscopy (TEM) measurements have evidenced we have pseudo smooth interfaces with terrace sizes smaller than the exciton Bohr diameter.

Therefore, in analogy with the GaAs(Ga,Al)As situation discussed above, we expect and we observe sharp asymmetric transition since the exciton samples wells have in-plane modulated thickness. As a consequence of this, the exciton samples a crystal that displays ordering in the growth direction and interfacial in-plane disorder. A localization phenomenon is responsible for the existence of the low energy photoluminescence wing. The exciton population in this wing is ruled by competition between radiative recombination and excitation transfer mechanisms (nonradiative processes) toward low energy levels in an exponential tail of density of states below the near band edge free exciton continuum as shown in Fig. 3. This phenomenon has been extensively described in bulk semiconductor alloys since the pioneering works of Permogorov et al.[25] and Cohen and Sturge[26] on exciton localization to potential fluctuation. Similar studies also appeared later and have enabled us to elucidate the nature of the photoluminescence in GaAs-AlAs type II short period superlattices.[27] We are confronted with a similar problem here. The intimate details of this physics are rather sophisticated to elucidate since various ingredients including existence of mobility edge, percolation processes, multiple range hopping transfer, etc. contribute to the phenomenon, and sometimes have to be included in the theory. This depends essentially on the strength of the potential fluctuation (extension and depth), and on its distribution between valence and conduction states. A recent description of the effect together with fitting computation has been proposed by Ouadjaout and Marfaing for II-VI mixed solid solutions.[28]

Due to the growth process we retained, our superlattices have smooth interfaces, i.e. the interdiffusion is small at the hetero-interfaces, and we have a situation close to the photoluminescence of sulfur-rich ZnSSe alloys:[29] the strength of the defects at the hetero-interfaces is sufficient to trap the excitons at low temperature. The amount of interface disorder rules the width of the 2K photoluminescence. This is consistent with lifetime measurements of the excitons in such samples which evidenced that the exciton lifetime is in relation with the coexistence of radiative and nonradiative recombination mechanisms.[14] Figure 4 displays a typical series of spectra taken for temperatures ranging between liquid helium temperature and 150K. Increasing the lattice temperature favors nonradiative processes with re-

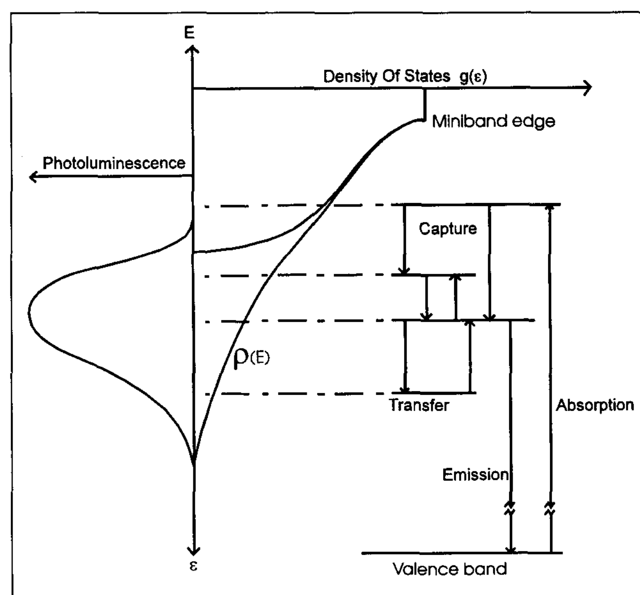

Fig. 3. Illustration of the competition between capture, transfer mechanisms which give the resulting population and the photoluminescence recombination band. On the figure, the energy of the incident photon is such that the absorption occurs in the middle of the exciton miniband.

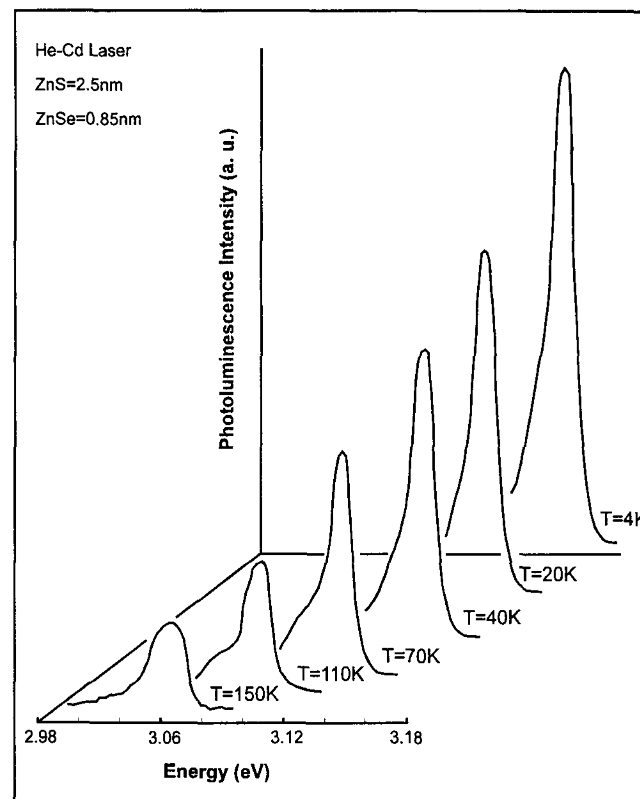

Fig. 4. Typical photoluminescence spectra which illustrate the temperature dependence of the photoluminescence of the ZnS-ZnSe superlattices.

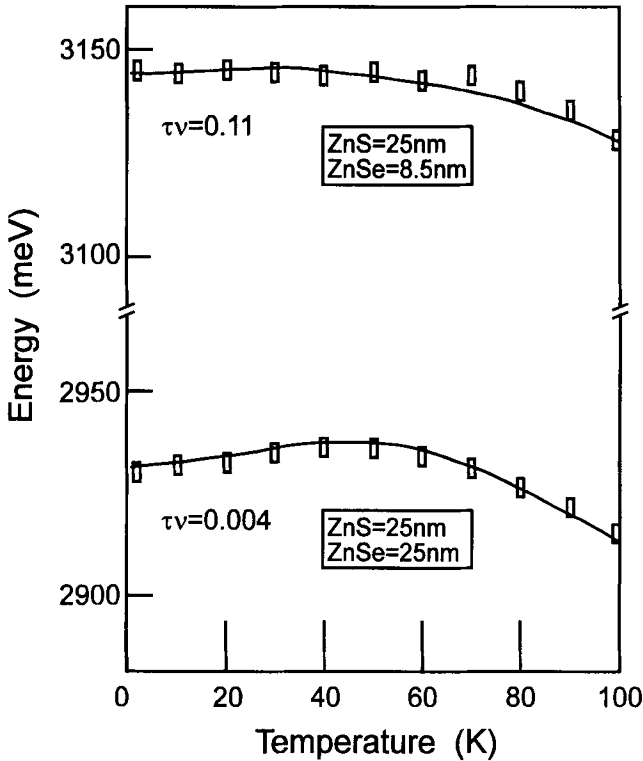

Fig. 5. Evolution of the photoluminescence maximum as a function of the lattice temperature. Full lines represent the result of the fitting procedure using the model described in the text, squares are experimental data.

spect to radiative recombination and we report observation of a decrease of the photoluminescence intensity. This behavior has been universally obtained on all our samples and is not peculiar to the physics of ZnS-ZnSe superlattices.

Figure 5 gives more intimate information concerning the different behaviors of the maximum of the photoluminescence peak in each superlattice when the temperature is changed. Data corresponding to different superlattices appear through utilization of symbols like squares. We note the *possible* occurrence of a shift of the photoluminescence maximum toward the high energy region when the temperature increases up to 50K. Then the evolution of the photoluminescence maximum follows the bandgap behavior: we observe a red shift. For all samples in the range of temperatures higher than 50K, the asymmetrical shape disappears, the line broadens, and its intensity diminishes. This behavior of the temperature of the photoluminescence spectra with temperature is consistent with a model of transfer process between localized states in the tail of density of states (Fig. 3). In this model, one expects that any increasing of the lattice temperature may favor the excitation transfer toward high energy localized states of the exponential tail of Fig. 3 via acoustic phonon absorption processes (thermal activation). When the thermal energy is sufficient, excitons no longer undergo the influence of potential fluctuations and then become delocalized (become free). These ideas have been completed by using a model where the low temperature high energy side of the photoluminescence peaks behaves like a mobility edge. In the spirit of this simplified model previously developed by Oueslati et al.,[30] we assume the spectral distribution of the photoluminescence intensity to be described by equation:

$$I(E,T) = \rho(E - Eg)\tau_{tot}(E,T)/\tau_{rad} \quad (1)$$

Where we have assumed for the sake of the simplicity that the radiative recombination rate τ_{rad} is independent of temperature T and energy E, which is a fairly good approximation. Next, from Ref. 14, we take $<\tau_{tot}(E,0)>\sim 100$ picoseconds). Finally, if we assume that, for temperature above T = 0K, the nonradiative depopulation mechanism τ_{nonrad} behaves like thermal excitations from E to an average critical value E_c at which the particles become mobile and may recombine (E_c can be compared to a genuine mobility edge), we can write in this model:

$$(\tau_{tot}(E,T))^{-1} = <\tau_{tot}(E,0)>^{-1} + \nu \exp[(E - E_c - E_g)/kT] \quad (2)$$

The nonradiative lifetime in Eq. (2) increases rapidly when E decreases since the exciton state is more localized, and the density of state available decreases. In analogy with the analysis of the problem for bulk semiconductor alloy systems, the density of states $\rho(E)$ that appears in Eq. (1) and on Fig. 3 is taken as: $\rho(E) = \exp((E - Eg)/E_o)a(E)$ where E_o is the average localization energy for the exciton.[26] The temperature dependence of the superlattice band gap E_g has been expressed following O'Donnel et al.,[31] using the following equation where Γ_1 is the electron-phonon coupling energy and $<\hbar\omega>$ is an adapted phonon energy:

$$Eg(T) = E_g(0) - \Gamma_1 [\coth(<\hbar\omega/2kT) - 1] \quad (3)$$

Results of the fitting appears on Fig. 5, full lines. We note the excellent agreement between the theory and the experiment, and in particular that the localization energy we obtain from the photoluminescence line shape fitting using a(E) = 1 like in Ref. 26 in the expression of the tail of states in Eq. (1), (some 36 meV), is comparable to values given by comparable analysis on weakly disordered semiconductors. We note in particular that the fitting is a very sensitive function of a(E) and we note that using a(E) = 3/2 like in Ref. 28 gives 10 meV. This illustrates one more time the difficulty of treating localization problems.[32] We have plotted on Fig. 6 the temperature dependence of the ratio between radiative and nonradiative lifetimes calculated at various energies of the photoluminescence band. Obviously, the radiative processes dominate the low temperature recombination process. The last point we want to make concerns the mobility edge energy E_C. The value we used in the fitting procedure is 10 meV. This value is some four times smaller than the average value of the localization energies we obtained in our samples. We believe this indicates that thermal quenching of the photoluminescence of such ZnS-ZnSe SLSs cannot be ruled by a thermal activation energy associated with ther-

mal dissociation of the free exciton into free electron-hole pair as previously claimed in the literature.[8,9]

ELECTRONIC STRUCTURE

To bring additional arguments along this line, we have calculated the exciton binding energy in our samples. Before doing that, we have performed an envelope function calculation of the electronic structure of the type I superlattices. Our data has been found consistent with a model where the total conduction band offset is small (some 80 meV) compared with the heavy-hole one (~800 meV). This conduction band offset can be divided into a constant strain free contribution of 220 meV and a strain dependent one. As the superlattices are in a strain state where the elastic energy has been minimized, the strain dependent quantity can be subject of slight variations depending whether the layers are in tensile or compressive stress situation.[6] This appears on Table I where we have reported the electron, heavy-hole, light-hole confining potentials V_i and miniband dispersions Δ_i. All these quantities are expressed in meV. Our results match with the most accurate data reported in the literature (This is reviewed in Ref. 6).

The Coulomb interaction is important in wide gap bulk II-VI semiconductors. As in all type I low-dimensional systems, the confinement should increase this binding energy.[33] This interaction may even exceed the energy of the LO phonon (~31.3 meV in ZnSe). We have calculated it in the context of the variational approach using different trial functions in case of an isolated quantum well. In cylindrical coordinates, the hamiltonian writes:

$$H = H_e + H_v + H_{ex}$$

$$H_{ex} = -\frac{\hbar^2}{2\mu}\left(\frac{\partial^2}{\partial\rho^2}+\frac{1}{\rho}\frac{\partial}{\partial\rho}\right)-\frac{e^2}{4\pi\varepsilon_0\varepsilon_r\sqrt{\rho^2+z^2}}+\frac{1}{\rho^2}\frac{\partial^2}{\partial\theta^2}$$

The solutions of the electron and hole contributions H_e and H_v are the envelope functions for the electron and hole.

The eigen states of the Schrödinger equation E are: $E = E_e + E_h + E_b$. We have calculated the heavy-hole exciton binding energy. The exciton wave function is written as the product of the electron and hole envelope functions with an excitonic-like trial function. In cylindrical coordinates trial functions $\Phi_o(\rho,z_e,z_h)$ =

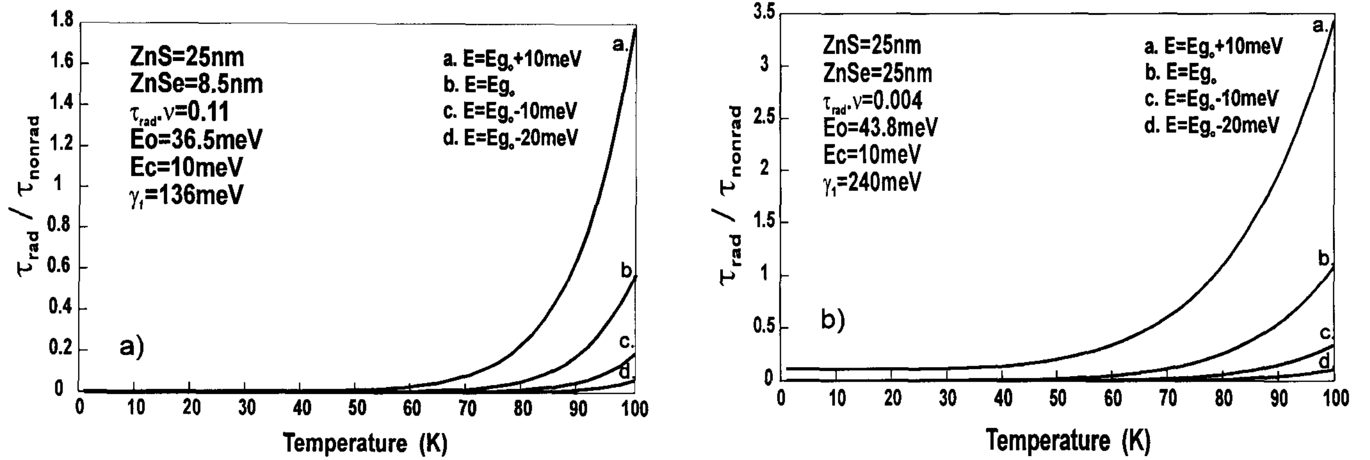

Fig. 6. Evolution of the ratio between radiative and nonradiative processes obtained from the fitting in case of two superlattices.

Table I. Results of the Envelope Function Calculation as a Function of the Numbers of ZnS and ZnSe Monolayers

N_{ZnS}/N_{ZnSe}	Ve (meV)	Vhh (meV)	Vlh (meV)	Δe (meV)	Δhh (meV)	Δlh (meV)
3/3	83.1	834.5	615.1	519	33.5	302
3/6	83.5	824.1	604.3	228	6.1	91
3/9	83.7	818.5	597.7	132	2.3	41
6/3	82.8	844.1	623.2	212	2	80
6/6	83.1	834.5	615.1	116.17	0.3	22.4
6/9	83.3	828.3	609	72	0.1	9.4
9/3	82.6	848.6	626.4	113	0	22.8
9/6	82.9	840.3	620.3	64	0	4.8
9/9	83.1	834.5	615.1	41	0	1.8

Note: See text for details.

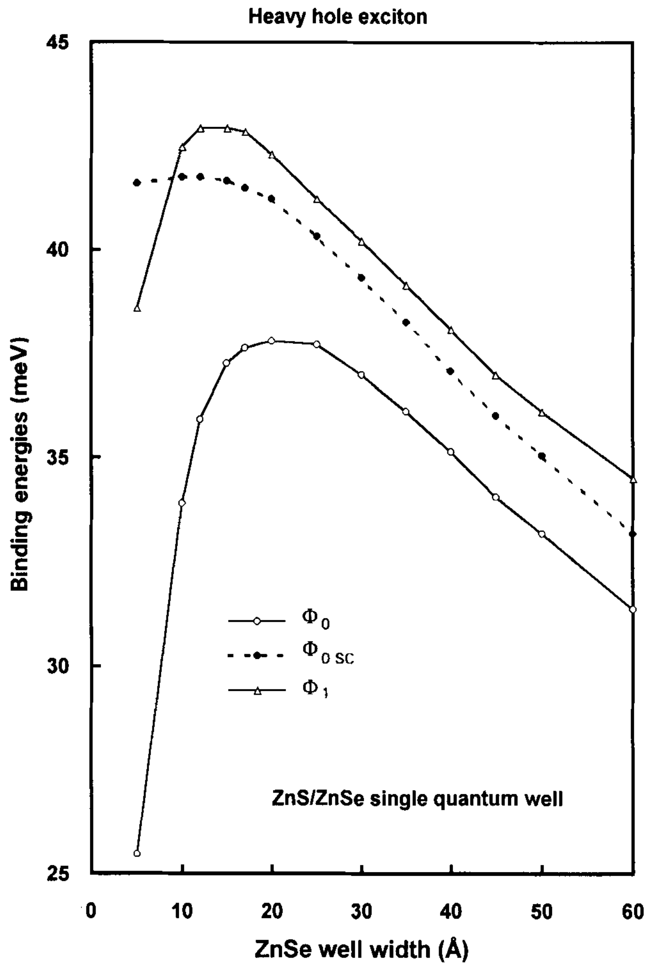

Fig. 7. The heavy-hole exciton binding energy calculated using three different models. See text for details.

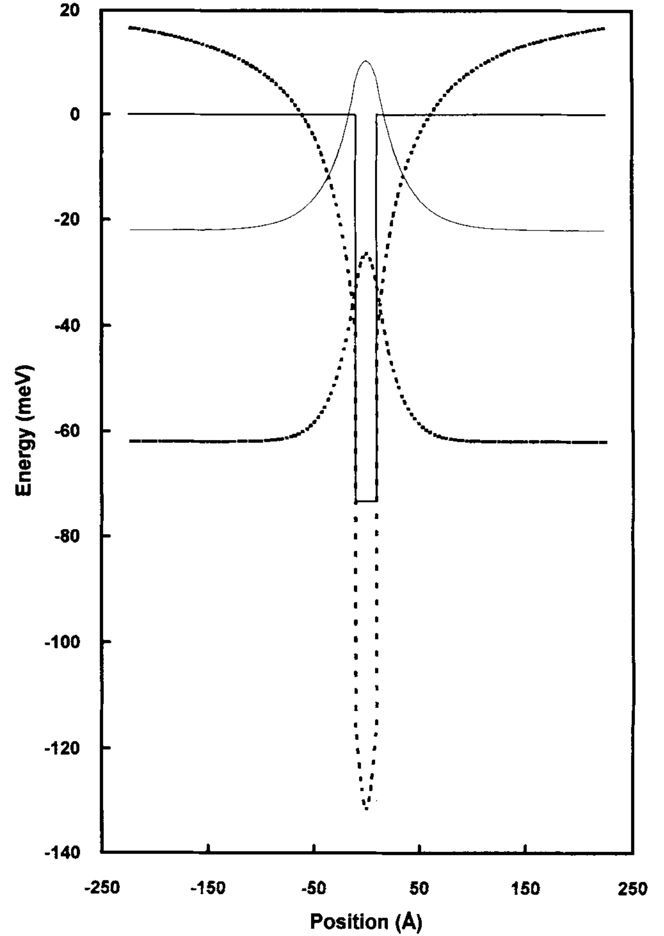

Fig. 8. Zero-order conduction line-up and electron envelope function (full lines) calculated for a 20Å ZnSe well. The results of the self-consistent variational calculation of the conduction line-up and electron envelope function are represented using dashed lines. The envelope functions are shifted from the value of the self-consistent heavy-hole exciton.

$\exp(-\rho/\lambda)$, and $\Phi_1(\rho,z_e,z_h)=\exp\left(-\sqrt{\rho^2+\alpha^2(z_2-z_h)^2}/\lambda\right)$ have been used. Parameters λ and α are variational parameters. The result of the calculation appears in Fig. 7. For these finite wells, the second trial function is much more appropriate than the simplest one, particularly for large ZnSe layers.

As the binding energy may be important compared to the electron confining potential, the expansion of the exciton wave function as the product of the electron and hole envelope functions solutions of a square well problem, with an excitonic-like trial function might not be appropriate since the localized hole wave function could deform the electron confining potential. This has been demonstrated for type II band line-ups with marginal valence potentials like (Ga, In)As-GaAs,[34] CdTe-(Cd,Zn)Te,[35] or CdTe- (Cd,Mn)Te.[36,37] The resolution of the problem requires one to perform a self-consistent calculation. We now adopt a more sophisticated formalism to describe the exciton. We write the total exciton wave function:

$$\Phi(z_e,z_h,\rho)=\sqrt{\frac{2}{\pi\lambda^2}}\chi_h(z_h).f(z_e).e^{-\rho/\lambda}$$

with $f(z_e)$ being the self-correcting electron eigenfunction, satisfying a Schrödinger equation in which the potential term $V_e'(z_e)$ includes the interaction with the hole:

$$\left(-\frac{\hbar^2}{2m_e}\frac{\partial^2}{\partial z_e^2}+V_e'(z_e)\right)f(z_e)=(E_e+E_b).f(z_e)$$

$$V_e'(z_e)=$$

$$V_e(z_e)+\frac{\hbar^2}{2\mu\lambda^2}-\frac{e^2}{4\pi\varepsilon_0\varepsilon_r}\left(\frac{2}{\lambda}\right)^2\int_{-\infty}^{+\infty}\chi_h^2\,dz_h\int_0^{\infty}\frac{e^{-2\rho/\lambda}\rho\,d\rho}{\sqrt{\rho^2+z_{eh}^2}}$$

The result of this third calculation also appears in Fig. 7. This calculation gives intermediate values but seems more appropriate than Φ_1 for the case of wide wells since it tends more rapidly toward a bulk ZnSe-like value. As the envelope function for the electron is obtained from the knowledge of the heavy-hole one, this self-consistent calculation, which avoids the tedious calculations required to treat the exciton interaction in superlattices, is extremely reasonable for superlattices which exhibit electron miniband dispersion and no tunneling of the hole wave function between adjacent wells which is the case of our superlattices. Figure 8 displays the modification of the conduction potential and electron envelope function we have obtained from this self-consistent calcu-

lation for a 2 nm ZnSe well. The self-consistent data are shown using dashed lines. We note that the corrected electron eigenfunction spreads less due to the strong correction (more than 60 meV) on the electron confinement energy. This makes such superlattices very interesting for theoretical investigations, like any low dimensional system (quantum wells, superlattices) that exhibits a marginal potential in the valence or conduction band. To conclude, we wish to emphasize the fact that the Rydberg energies are larger than the average extension of the low energy photoluminescence tail of the high energy peak of the photoluminescence spectra. This means that localization effects due to potential fluctuations can be easily counterbalanced by increasing the sample temperature. The exciton remains stable at room temperature.

CONCLUSION

High quality ZnS-ZnSe short period superlattices have been grown by MOVPE using a novel zinc adduct precursor TMMD:DMZ. We have made a series of photoreflectance experiments completed by envelope function calculation of the band structure. These data have been completed by variational and self-consistent variational calculation of the Rydberg energies. These values have been compared with the average localization energy of the exciton to interfacial potential fluctuations which we deduce from the lineshape of the photoluminescence. Moreover, the temperature dependence of the photoluminescence shows that nonradiative transfer processes in the tail of potential fluctuation behaves like a mobility edge and compete with the radiative recombination processes.

ACKNOWLEDGMENTS

This work is partly supported by the Commission of the European Communities under contract ESPRIT-BASIC RESEARCH MTVLE 6675 and contract HCM No. ERBCHRX-CT93-0321. The Groupe d'Etude des Semiconducteurs is Unité de Recherche Associée au CNRS No. 357.

REFERENCES

1. J.Y. Zhang, X.W. Fan, S.Y. Wang, D.Z. Shen and G.H. Fan, *J. Cryst. Growth* 117, 523 (1992).
2. X.W Fan, D.Z. Shen, J.Y. Zhang, Z.P. Guan and H. Tian, *Proc. 20th Intl. Conf. on the Physics of Semiconductors*, ed. E.M. Anastassakis and J.D. Joannopoulos, (Singapore: World Scientific, 1991), p. 1016.
3. T. Yokogawa, T. Saitoh and T. Narusawa, *Appl. Phys. Lett.* 58, 1754 (1991).
4. O. Briot, M. DiBlasio, T. Cloitre, N. Briot, P. Bigenwald, B. Gil, M. Averous, R.L. Aulombard, L.M. Smith, S.A. Rushworth and A.C. Jones, *Proc. MRS Mtg.*, San Fransisco 1994, vol 340, (1994), p. 515.
5. D. Bouchara, A. Abounadi, M. DiBlasio, N. Briot, T. Cloitre, O. Briot, B. Gil, J. Calas, M. Averous and R.L. Aulombard, *J. Crystal Growth* 138, 121 (1994).
6. B. Gil, T. Cloitre, M. DiBlasio, P. Bigenwald, L. Aigouy, N. Briot, O. Briot, D. Bouchara, R.L. Aulombard and J. Calas, *Phys. Rev B* 50, (Dec. 15, 1994).
7. H. Kuwabara, H. Fujiyasu, H. Shimizu, A. Sasaki and S. Yamada *J. Cryst. Growth* 72, 299 (1985); T Yokogawa, M. Ogura and T. Kajiwara, *Appl. Phys. Lett.* 49, 1702 (1986).
8. T. Yokogawa, M. Ogura and T. Kajiwara, *J. Appl. Phys.* 62, 2843 (1987); T. Yokogawa, T. Fujita, M. Ogura and T. Kajiwara, *J. Cryst. Growth* 93, 708 (1988); T. Yokogawa, H. Sato and M. Ogura, *J. Appl. Phys.* 64, 5201 (1988); T. Yokogawa, T. Saitoh and T. Narasawa, *J. Cryst. Growth* 101, 550 (1990).
9. Y. Yamada and T. Taguchi, *J. Cryst. Growth* 101, 661 (1990).
10. Y. Kawakami, T. Taguchi, A.Hiraki, Technology Reports of the Osaka University, vol 38–1921, p. 109-118, (1988), *J. Crystal Growth* 93, 714 (1988).
11. K.P. O'Donnell, P.J. Parbrook, B. Henderson, C. Trager-Cowan, X. Chen, F Yang, M.P. Halsall, P. J. Wright and B. Cockayne *J. Cryst. Growth* 101, 554 (1990).
12. T. Yao, M. Fujimoto, S.K. Chang and H. Tanino, *J. Cryst. Growth* 111, 823 (1991).
13. A. Shen, H. Wang, Z. Wang and S. Iu, *Appl. Phys. Lett.* 60, 2640 (1992).
14. J. Cui, H. Wang, F. Gan, X. Huang, Z. Cai, Q. Li and Z. Yu, *Appl. Phys. Lett.* 61, 1540 (1992).
15. F. Yang, P.J. Parbrook, B. Henderson, K.P. O'Donnell, P.J. Wright and B. Cockayne, *Appl. Phys. Lett.* 59, 2142 (1991); K.P. O'Donnell, P.J. Parbrook, F. Yang, X. Chen, D.J. Irvine, C. Trager-Cowan, B. Henderson, P.J. Wright and B. Cockayne. *J. Cryst. Growth* 117, 497 (1992).
16. Z.P. Guan, J.H. Zhang, G.H. Fan and X.W. Fan, *J. Cryst. Growth* 117, 515 (1992).
17. J. Cui, H. Wang and F. Gan, *J. Cryst. Growth* 117, 505 (1992).
18. F.E.G. Guimaraes, J. Sollner, K. Marquardt, M. Heuken and K Heime, *J. Cryst. Growth* 117, 1075 (1992).
19. C. Pong, F. Feigelson and R.C. DeMattei, *J. Cryst. Growth* 128, 650 (1993).
20. S. Hohnoki, S. Katayama and A. Hasegawa, *Solid State Com.* 89, 41 (1994).
21. Shen Dezhen, Fan Xiwu and Fan Guanghan, *Chinese Physics* 12, 758 (1992).
22. Z.P. Guan, X.W. Fan, G.H. Fan and X/R. Xu, *J. Luminescence* 45, 224 (1990).
23. J. Massies, C. Deparis, C. Neri, G. Neu, Y. Chen, B. Gil, P. Auvray and A. Regreny, *Appl. Phys. Lett.* 55, 2605 (1989).
24. Y. Chen, J. Massies, G. Neu, C. Deparis and B. Gil, *Solid State Com.* 81, 877 (1992).
25. S. Permogorov, A. Reznitzky, S. Verbin, G.O. Muller, P. Flogel, M. Nikiforova, *Phys. Stat. Solidi* B113, 589 (1982).
26. E. Cohen and M.D. Sturge, *Phys. Rev. B* 25, 3828 (1982).
27. D. Scalbert, J. Cernogora, C. Benoit à la Guillaume, M. Maaref, F.F. Charfi and R. Planel, *Solid State Com.* 70, 945 (1989).
28. D. Ouadjaout and Y. Marfaing, *Phys. Rev. B* 41, 12096 (1990); *Phys. Rev. B* 46, 7908 (1992).
29. L.G. Suslina, D.L. Fedorov, S.G. Konnikov, F.F. Kodzhespirov, A.A. Andreev and E.G. Sharlai, *Sov. Phys. Semicond.* 11, 1132 (1977); R. Mach, L.G. Suslina and A.C. Areshkin, *Sov. Phys. Semicond.* 16, 418 (1982).
30. M. Oueslati, M. Zouaghi, M.E. Pistol, L. Samuleson, H.G. Grimmeis and M. Balkanski, *Phys. Rev B* 32, 8220 (1985).
31. K.P. O'Donnel and X. Chen, *Appl. Phys. Lett.* 58, 2924 (1991).
32. Interesting results and interpretations may appear as in X. Chen, B. Hendreson and K.P. O'Donnel, *Appl. Phys. Lett.* 60, 2672 (1992).
33. G. Bastard, E.E. Mendez, L.L. Chang and L. Esaki, *Phys. Rev. B* 26, 1974 (1982); R.L. Greene and K.K. Bajaj, *Solid State Com.* 45, 831 (1983); R.L. Greene, K.K Bajaj and D.E. Phelps, *Phys. Rev. B* 29, 1807.
34. P. Bigenwald and B. Gil, *Solid State Com.* 91, 33 (1994).
35. E. Deleporte, G. Peter, J.M. Berroir and C. Delalande, *Surf. Sci.* 267, 137 (1992).
36. G. Peter, E. Deleporte, G. Bastard, J.M. Berroir, C. Delalande, B. Gil, J.M. Hong and L.L. Chang, *J. Luminescence* 52, 147 (1992); E. Deleporte, J.M. Berroir, G. Bastard, C. Delalande, J.M. Hong and L.L. Chang, *Phys. Rev. B* 42, 5891 (1990).
37. S.K. Chang, A.V. Nurmikko, J.W. Wu, L.A. Kolodziejski and R.L. Gunshor, *Phys. Rev. B* 37, 1191 (1988).